Journal of Sound and Vibration 330 (2011) 1196–1210

Contents lists available at ScienceDirect

Journal of Sound and Vibration

journal homepage: www.elsevier.com/locate/jsvi

Structural health monitoring and damage assessment using a novel time series analysis methodology with sensor clustering

Mustafa Gul, F. Necati Catbas*

Department of Civil, Environmental and Construction Engineering, University of Central Florida, USA

ARTICLE INFO

Article history:
Received 13 December 2009
Received in revised form
1 September 2010
Accepted 23 September 2010
Handling Editor: I. Trendafilova
Available online 18 October 2010

ABSTRACT

This study presents a novel time series analysis methodology to detect, locate, and estimate the extent of the structural changes (e.g. damage). In this methodology, ARX models (Auto-Regressive models with eXogenous input) are created for different sensor clusters by using the free response of the structure. The output of each sensor in a cluster is used as an input to the ARX model to predict the output of the reference channel of that sensor cluster. Two different approaches are used for extracting Damage Features (DFs) from these ARX models. For the first approach, the coefficients of the ARX models are directly used as the DFs. It is shown with a 4 dof numerical model that damage can be identified, located and quantified for simple models and noise free data. To consider the effects of the noise and model complexity, a second approach is presented based on using the ARX model fit ratios as the DFs. The second approach is first applied to the same 4 DOF numerical model and to the numerical data coming from an international benchmark study for noisy conditions. Then, the methodology is applied to the experimental data from a large scale laboratory model. It is shown that the second approach performs successfully for different damage cases to identify and locate the damage using numerical and experimental data. Furthermore, it is observed that the DF level is a good indicator for estimating the extent of the damage for these cases. The potential and advantages of the methodology are discussed along with the analysis results. The limitations of the methodology, recommendations, and future work are also addressed.

1. Introduction

Structural Health Monitoring (SHM) is the research area focusing on condition assessment of different types of structures including aerospace, mechanical and civil structures. Damage detection is arguably one of the most critical components of SHM. Identifying the presence of the damage (structural or material change that affects the behavior of the structure adversely) might be considered as the first step to take preventive actions and to start the process towards understanding the root causes of the problem.

Various methodologies have been proposed for detecting damage using SHM data. For global condition assessment, most of these methodologies employ vibration data by using one or a combination of different time domain and/or frequency domain algorithms. The aim is to extract features that will be sensitive to the changes occurring in the structure and relatively insensitive to other interfering effects (e.g. operational and environmental effects). Some of these methodologies can be found in literature and the references therein [1–5].

* Corresponding author. Tel.: +1 407 823 3743.
E-mail address: Catbas@mail.ucf.edu (F.N. Catbas).

0022-460X/$ - see front matter © 2010 Elsevier Ltd. All rights reserved.
doi:10.1016/j.jsv.2010.09.024

One common approach to extract damage sensitive features (or damage features) from SHM data is to use *time series analysis*. These types of methods have gained considerable attention recently since their implementation for an automated SHM system is relatively more feasible compared to other methodologies such as damage detection based on model updating. Most of the time series analysis based methodologies aim to fit time series models to the vibration data and then try to detect the damage by extracting damage features from these time series models. Some of these methodologies directly compare the time series models whereas some of them use the residual errors when the new data is used with the previously created model. These methodologies usually make use of AR (Auto-Regressive), ARX (Auto-Regressive models with eXogenous outputs) and/or ARMA (Auto-Regressive Moving Average) models to detect the damage in a statistical manner [5–16]. Although these methodologies are generally successful in identifying the presence of the damage (i.e. level 1 damage identification as defined by Rytter [17]), most of them give limited information about the location and/or severity of the damage (i.e. level 2 and/or level 3 damage identification). For example, Sohn et al. [7] demonstrated the early examples of time series analysis and outlier analysis based damage detection. The researchers used AR and ARX models in conjunction with Mahalanobis distance based outlier detection to find the damage. They were successful at identifying the presence of the damage however; no information was obtained about the location or severity of the damage. Different versions of time series models were also used by different researchers for damage detection. For example, Nair et al. [16] used an ARMA model and used the first three AR components as the damage sensitive feature and they were able to identify and locate the damage. In another study, Omenzetter and Brownjohn [8] used Auto-Regressive Integrated Moving Average (ARIMA) models to analyze the static strain data from a bridge during construction and when it was opened to service. Although the authors were able to detect structural changes with the methodology, they also acknowledged that the location and severity of the damage could not be identified.

Lu and Gao [18] used a modified ARX model for damage identification and localization. The acceleration response at one location was chosen as the input to their ARX model to predict the outputs at the other locations of the structure. In that study, an ARX model is created for the healthy structure. Then the same model is used to predict the outputs of the damaged structure. The residual error of the model reflects the structural change and the standard deviation of the residual error is selected as the damage sensitive feature. The researchers used two shear-type numerical spring mass models for verification of the methodology and showed that their approach was successful for identification and localization of the damage in those models for noise free data. In another study, a similar methodology was adapted by Monroig and Fujino [19] where the researchers used a second-order multivariate ARX models with simulated data (with 1% additional noise) coming from a building model. They showed that the methodology was able to identify and locate the damage although there are some false-positive and false negative results.

As summarized above, time series modeling has a great potential for damage detection applications. However, there is still a need for time series analysis methodologies for three levels of damage detection. In this study, a robust and practical damage identification methodology is presented by using time series analysis. The novelty of the proposed method compared to the most of the methodologies in the literature is that damage can be identified, located by using only free response output data with a practical and easy to automate approach without any need of excitation information. Furthermore, the proposed damage feature is a good indicator for estimating the extent of the damage. ARX models are created for different sensor clusters and different damage sensitive features are extracted from these models. These features are then used for identifying, locating and estimating the extent of the damage. It should be noted however, that establishing a direct relationship between the damage features and the stiffness reduction is beyond the scope of this study.

Two different approaches based on ARX models are presented. First, the theoretical basis and background of these two approaches are explained. Then the methodology is applied to different numerical and experimental data. A 4 DOF numerical model and a numerical benchmark problem using a complex finite element model of an existing laboratory structure were employed for the numerical investigations. The experimental studies were conducted by using a steel grid type large-scale laboratory model. The analysis results are presented along with the discussions about the advantages and disadvantages of the methodology. Finally, the directions for future research before the methodology can be used in real life are discussed.

2. Structural dynamics and time series modeling

2.1. General formulations: structural dynamics

The equation of motion for an N degrees of freedom (dof) linear dynamic system can be written in matrix form as in Eq. (1):

$$\begin{bmatrix} m_{11} & \cdots & m_{1N} \\ \vdots & \ddots & \vdots \\ m_{N1} & \cdots & m_{NN} \end{bmatrix} \begin{Bmatrix} \ddot{x}_1 \\ \vdots \\ \ddot{x}_N \end{Bmatrix} + \begin{bmatrix} c_{11} & \cdots & c_{1N} \\ \vdots & \ddots & \vdots \\ c_{N1} & \cdots & c_{NN} \end{bmatrix} \begin{Bmatrix} \dot{x}_1 \\ \vdots \\ \dot{x}_N \end{Bmatrix} + \begin{bmatrix} k_{11} & \cdots & k_{1N} \\ \vdots & \ddots & \vdots \\ k_{N1} & \cdots & k_{NN} \end{bmatrix} \begin{Bmatrix} x_1 \\ \vdots \\ x_N \end{Bmatrix} = \begin{Bmatrix} f_1 \\ \vdots \\ f_N \end{Bmatrix} \tag{1}$$

where m_{ij} is the mass, c_{ij} is the damping and k_{ij} is the stiffness coefficients. The vectors $\ddot{x}_i$, $\dot{x}_i$ and x_i are acceleration, velocity and displacement for the ith dof, respectively. The external forcing function on the system is denoted with f_i.

The equality in Eq. (2) is obtained if the first row of Eq. (1) is written separately. By rearranging Eq. (2), it is seen that the output of the 1st dof can be written in terms of the excitation force on 1st dof, the physical parameters of the structure, and the outputs of the other dofs (including itself). Furthermore, in case of free response, the force term can be eliminated and the relation is written as shown by Eq. (3):

$$(m_{11}\ddot{x}_1+\cdots+m_{1N}\ddot{x}_N)+(c_{11}\dot{x}_1+\cdots+c_{1N}\dot{x}_N)+k_{11}x_1+\cdots+k_{1N}x_N=f_1 \tag{2}$$

$$\ddot{x}_1=-\frac{(m_{12}\ddot{x}_2+\cdots+m_{1N}\ddot{x}_N)+(c_{11}\dot{x}_1+\cdots+c_{1N}\dot{x}_N)+(k_{11}x_1+\cdots+k_{1N}x_N)}{m_{11}} \tag{3}$$

It is seen from Eq. (3) that if a model is created to predict the output of the first dof by using the dofs connected to it (neighbor dofs), the change in this model can reveal important information about the change in the properties of that part of the system. Obviously, similar equalities can be written for each row and different models can be created for each equation. Each row of Eq. (1) can be considered as a sensor cluster with a reference dof and its neighbor dofs. The reference dof for Eq. (3), for example, is the first dof and neighbor dofs are the dofs that are directly connected to the first dof. Therefore, it is proposed that different linear time series models can be created to establish different models for each sensor cluster and changes in these models can point the existence, location and severity of the damage. The details of the methodology are explained in the following sections.

Note from the formulations that there are velocity and displacement terms in the equations. However, the time series models used in this study only incorporate acceleration output. Since the velocity and displacement of a system are not independent from its acceleration response, it is assumed the model is inherently counting for these responses. However, numeric integration may be used for a more detailed analysis in future studies so that the model can count for mass, damping and stiffness parameters separately.

2.2. Time series modeling

Time series modeling (or analysis) is statistical modeling of a sequence of data points that are observed in time. It has been used in many different fields including structural dynamics and system identification. In the following sections, a brief discussion about time series modeling is given. A more detailed discussion about the theory of the time series modeling is beyond the scope of this study and can be found in the literature. [20–22].

A linear time series model to represent the relationship of the input, output, and the error terms of a system can be written with the difference equation shown in Eq. (4) [21]. A more compact form of this equation is shown in Eq. (5):

$$y(t)+a_1y(t-1)+\cdots+a_{n_a}y(t-n_a)=b_1u(t-1)+\cdots+b_{n_b}u(t-n_b)+e(t)+d_1e(t-1)+\cdots+d_{n_d}e(t-n_d) \tag{4}$$

$$\mathbf{A(q)y(t)}=\mathbf{B(q)u(t)}+\mathbf{D(q)e(t)} \tag{5}$$

where, **y(t)** is the output of the model, **u(t)** is the input to the model, and **e(t)** is the error term. The unknown parameters of the model are shown with a_i, b_i, and d_i and the model orders are shown with n_a, n_b, and n_d. **A(q)**, **B(q)**, and **D(q)** in Eq. (5) are polynomials in the delay operator q^{-1} as shown below in Eq. (6). The model shown in Eq. (5) can also be referred as an ARMAX model (Auto-Regressive Moving Average model with eXogenous input) and a block diagram of an ARMAX model can be shown as in Fig. 1(a):

$$\begin{aligned}\mathbf{A(q)}&=1+a_1q^{-1}+a_2q^{-2}+\cdots+a_{n_a}q^{-n_a}\\ \mathbf{B(q)}&=b_1q^{-1}+b_2q^{-2}+\cdots+b_{n_b}q^{-n_b}\\ \mathbf{D(q)}&=1+d_1q^{-1}+d_2q^{-2}+\cdots+d_{n_d}q^{-n_d}\end{aligned} \tag{6}$$

By changing the model orders of an ARMAX model, different types of time series models can be created. For example, if $n_b=n_d=0$, the model is referred as an AR model, whereas an ARMA model is obtained by setting n_b to zero. In this study, the model orders are non-zero for **A(q)** and **B(q)** terms, i.e. ARX models are used. The structure of an ARX model is shown

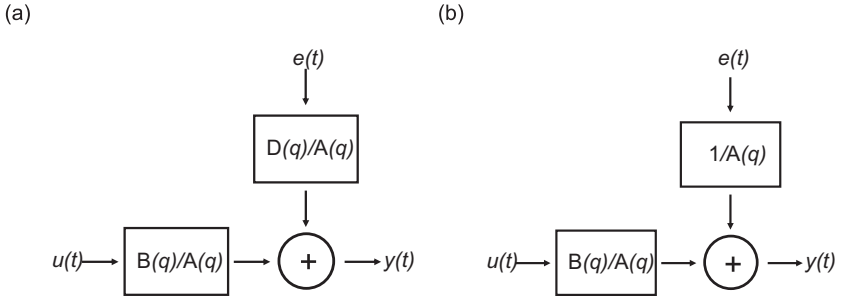

Fig. 1. The block diagram of (a) an ARMAX and (b) ARX model (adapted from [20]).

in Eq. (7) whereas the block diagram of the model is shown in Fig. 1(b).

$$\mathbf{A(q)y(t)} = \mathbf{B(q)u(t)} + \mathbf{e(t)} \tag{7}$$

2.3. Creating the ARX models for different sensor clusters

The core of the methodology presented in this study is to create different ARX models for different sensor clusters and then extract damage sensitive features from these models to detect the damage. In these ARX models, the **y(t)** term is the acceleration response of the reference channel of a sensor cluster, while the **u(t)** term is the acceleration responses of all the dofs in the same cluster. Eq. (8) shows an example ARX model to estimate the 1st dof's output by using the other dofs' outputs for a sensor cluster with k sensors.

$$\mathbf{A(q)}\ddot{\mathbf{x}}_{\mathbf{1}}(t) = \mathbf{B(q)}\left[\ddot{\mathbf{x}}_{\mathbf{1}}(t)\ddot{\mathbf{x}}_{\mathbf{2}}(t)\cdots\ddot{\mathbf{x}}_{\mathbf{k}}(t)\right]^{\mathbf{T}} + \mathbf{e(t)} \tag{8}$$

To explain the methodology schematically, a simple 3-dof model is used as an example. Fig. 2(a) shows the first sensor cluster for the first reference channel. The cluster includes first and second dofs since the reference channel is connected only to the second dof. The input vector **u** of the ARX model contains the acceleration outputs of first and second dofs. The output of the first dof is used as the output of the ARX model as shown in the figure. When the second channel is the

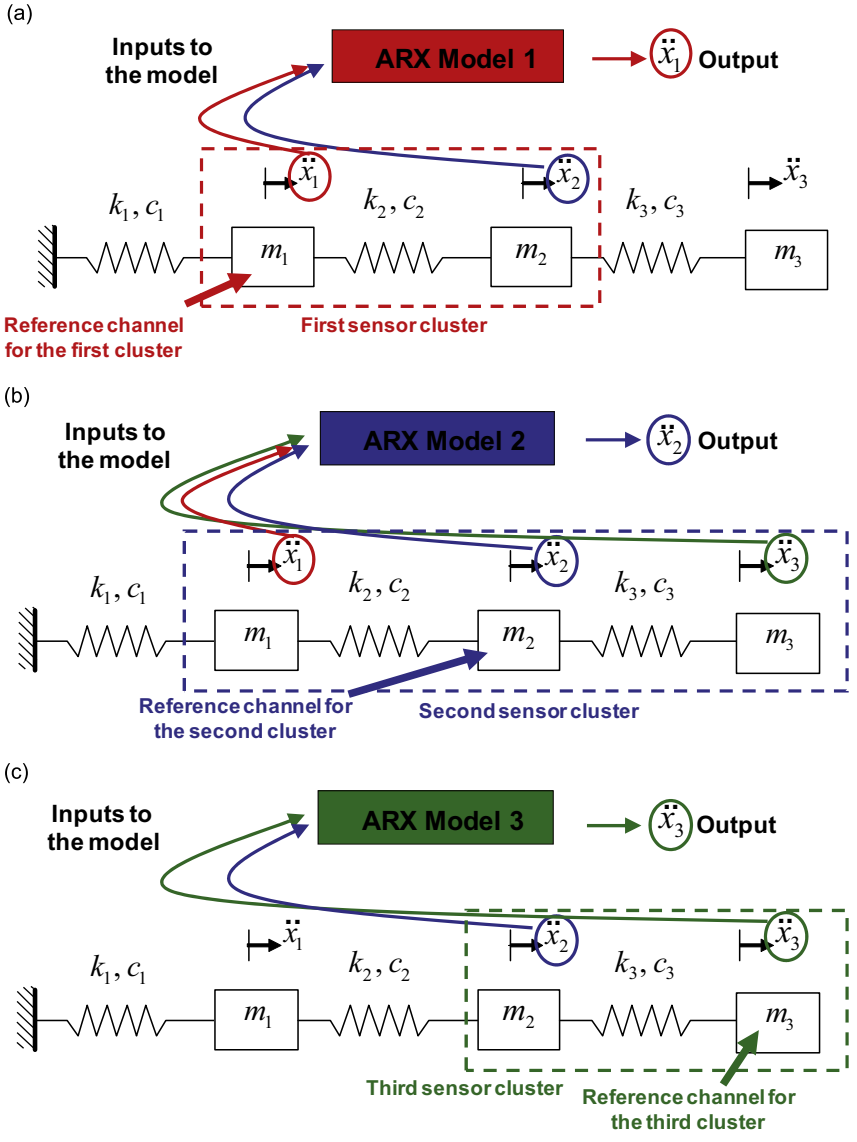

Fig. 2. Creating different ARX models for each sensor cluster (a) first sensor cluster, (b) second sensor cluster, and (c) third sensor cluster.

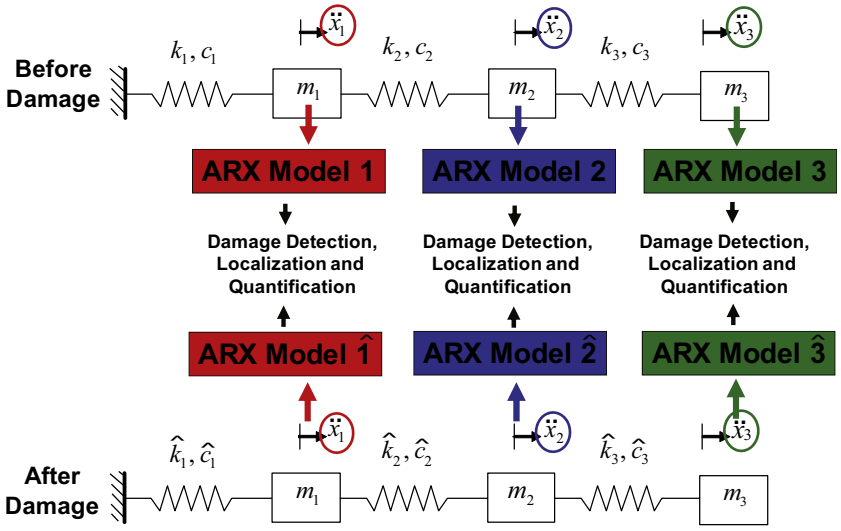

Fig. 3. Comparing the ARX models for each sensor cluster for damage assessment.

reference channel, Fig. 2(b), the sensor cluster includes all three dofs since they are all connected to the second dof. The outputs of the first, second, and third dofs are used as the input to the ARX model and then the output of the second dof is used as the output of this model. Likewise, for the reference channel three (Fig. 2 (c)), the inputs to the ARX model are the output of the second and third channels and the output of the model is the third channel itself.

After creating the ARX models for the baseline condition, two different approaches are presented for detecting damage. Approach I is based on the assumption that the comparison of the ARX models for each sensor cluster before and after damage (Fig. 3) will give information about the existence, location, and severity of the damage. For Approach II, the fit ratios of the baseline ARX model when used with new data is employed as a damage sensitive feature. The details about the two approaches and damage features are presented in the next sections.

3. Approach I: ratio of the ARX model coefficients as a damage feature (DF)

As explained in the previous sections, two different approaches are used for comparison of the ARX models, i.e. two different damage features (DFs) are extracted from these models. For Approach I, the *B* term coefficients of the ARX models are selected as the DFs [23]. It is shown that the change in these coefficients can be attributed directly to the stiffness change in the structure for simple and noise free models. This practical analysis gives exact identification, localization, and quantification of damage. However, it is also shown that when there is noise in the data, this approach will not work as it is and it needs to be modified.

3.1. 4 dof spring mass system

For verification of the Approach I, it is applied to a numerical 4 dof system. The system is shown in Fig. 4 and its properties can be summarized as: $m_1=0.8$, $m_2=2$, $m_3=1.2$, $m_4=0.6$, $k_1=20$, $k_2=10$, $k_3=15$, $k_4=10$, and $k_5=25$. The damping matrix is defined as $\mathbf{C}=0.001\times\mathbf{M}+0.0001\times\mathbf{K}$. The structural system being used in this study is very similar to the system that was used by Lus et al. [24].

First, the free response (acceleration) of the healthy system is simulated. Then four ARX models are created for four sensor clusters for the baseline case. The model orders for the ARX models are selected as n_a=1 and n_b=2. Since it is a simple model without any noise in the data, these model orders are sufficient to obtain a very accurate model. The damage simulations and results are discussed in the following sections.

3.1.1. Case 1-1: 10% stiffness reduction at k_3 (k_3=13.5), noise free data

For this damage scenario, the stiffness coefficient of the spring between m_2 and m_3 is reduced by 10% (k_3=13.5). Then, four new ARX models are created as it was done for the baseline case. The model orders are kept same, i.e. n_a=1 and n_b=2. The **B** term coefficients of each ARX model of the damaged structure are compared to the counterparts obtained with the baseline data. The results are shown in Table 1.

The first row of the table shows the change in the mean of the **B** term coefficients (there are two **B** term coefficients since the n_b=2) of the ARX model for the first sensor cluster. The 'n/a' in the fourth column of the first row indicates that fourth dof is not included in the first sensor cluster. Looking at the table, it is observed that the DFs between m_2 and m_3 has

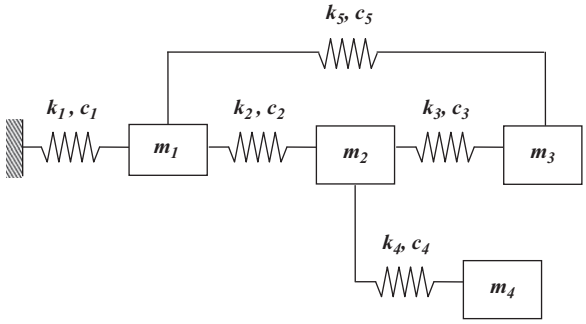

Fig. 4. The numerical model to generate data from simulations (similar to the model used in Lus et al. [24]).

Table 1
DF change (%) with respect to location when k_3=13.5 (10% stiffness loss between dofs 2 and 3).

Measurement location	dof 1	dof 2	dof 3	dof 4
dof 1	0.00	0.00	0.00	n/a
dof 2	0.00	0.00	−10.00	0.00
dof 3	0.01	**−10.00**	0.00	n/a
dof4	n/a	0.00	n/a	0.00

Table 2
DF change (%) with respect to location when k_3=13.5 (10% stiffness loss) with 5% noise added to the simulation data.

Measurement location	dof 1	dof 2	dof 3	dof 4
dof 1	65.94	952.78	195.45	n/a
dof 2	−4.37	−15.10	−159.51	−671.44
dof 3	−57.04	−27.13	−21.27	n/a
dof 4	n/a	60.02	n/a	−9.21

decreased whereas the other coefficients have remained constant. Moreover, it is seen that the decrease is 10% indicating the extent of the damage exactly. The results shown in the table clearly indicate that the methodology was successful for identifying, locating, and quantifying the damage for the 4 dof system. Finally, note that there are no false positives, i.e. there is no change in DFs for other dofs.

3.1.2. Case 1-2: 10% stiffness reduction in k_3 (k_3=13.5), with 5% noise

Although very successful results have been obtained with noise free data, Approach I is not successful in identifying the damage when noise is present in the data. To show this handicap, Case 1-1 is now repeated with 5% artificial white noise added to the data. Table 2 shows that the DF changes give no meaningful information about the damage, its location or severity.

The results are shown in Table 2 do not improve by increasing the model order number although a better fit to the data is obtained. The unsuccessful results obtained by Approach I for noisy data might be caused by the fact that linear regression solution assumes that the data in the input and output matrices are noise free. Another solution technique may be used to obtain better results but it is not investigated in this study. Another disadvantage of Approach I is that it does not work properly for complex models Considering these shortcomings, it is clear that the methodology will have limitations in real life applications. Therefore, the researchers improved the Approach I to consider the effect of noise and model complexity. The modified approach is referred as Approach II and is discussed in the next sections.

4. Approach II: fit ratio of the data as a DF

For this approach, the first step of the methodology remains same, i.e. ARX models are created for each sensor cluster for the baseline case. Then these models are used to predict the output of the damaged structure for the same sensor clusters. The difference between the fit ratios of the models is used as the DF [25]. The fit ratio (FR) of an ARX model is calculated as

given in Eq. (9):

$$\text{Fit Ratio (FR)} = \left(1 - \frac{|\mathbf{y} - \hat{\mathbf{y}}|}{|\mathbf{y} - \overline{\mathbf{y}}|}\right) \times 100 \tag{9}$$

where $\mathbf{y}$ is the measured output, $\hat{\mathbf{y}}$ is the predicted output, $\overline{\mathbf{y}}$ is the mean of $\mathbf{y}$, and $|\mathbf{y}-\hat{\mathbf{y}}|$ is the norm of $\mathbf{y}-\hat{\mathbf{y}}$. The DF is calculated by using the difference between the FRs for healthy and damaged cases as given in Eq. (10):

$$\text{Damage Feature (DF)} = \frac{\text{FR}_{\text{healthy}} - \text{FR}_{\text{damaged}}}{\text{FR}_{\text{healthy}}} \times 100 \tag{10}$$

4.1. 4 dof spring mass-noise free and noisy data

The second approach is tried with the same numerical model used in the previous section. Different cases are created to show that Approach II is successful at identifying and locating damage as well as estimating the extent of the damage for noisy cases. The cases are explained below.

4.1.1. Determining the threshold

Before damage identification with noisy data, the threshold for the DFs under noisy conditions should be established so that the change in the DFs due to the noise can be separated from the change due to damage. To define the threshold level, a methodology similar to one used by Worden et al. [26] is adapted. For this case, 10% random noise is added to two healthy data sets separately. There is no additional damage applied to the structure. Then the change in the DF is computed. This process is repeated 1000 times independently to create a statistically meaningful threshold level. To create a 99.9% confidence level for the threshold, the 999th highest DF is selected as threshold. The threshold value is obtained as 0.5239. By calculating this threshold, we ensure that not every change in the DFs is attributed to damage. If the change in DFs is under the threshold level, this change could have been caused by noise in the data or by the damage.

4.1.2. Case 2-1: 10% stiffness loss in k_3 (k_3=13.5), with 10% noise

After setting up the threshold value, damage simulations are conducted. For this case, the stiffness value of the spring between m_2 and m_3 is decreased by 10% as in Case 1-1. In addition, 10% random white noise is added to the data. Then the DFs are calculated for each dof by using Approach II. This process is repeated independently 100 times. Fig. 5 shows that the highest DF values are obtained for dof 3 and it is considerably higher than the threshold value. Moreover, DFs for dof 2 are higher than the threshold value (except five points out 100). Finally, the DFs for dof 1 and dof 4 are under the threshold value for all the simulations. These results clearly show that there is a structural change and it is occurred close to dofs 2 and 3. This is consistent with the applied damage where the stiffness value between m_2 and m_3 is decreased by 10%. The change in the DFs for dof 3 is higher than dof 2 because dof 3 is connected to two other dofs and a change in one of those connections affects it more compared with dof 2, which is connected to three dofs. From this case, it is observed that damage is identified and located successfully for noisy data.

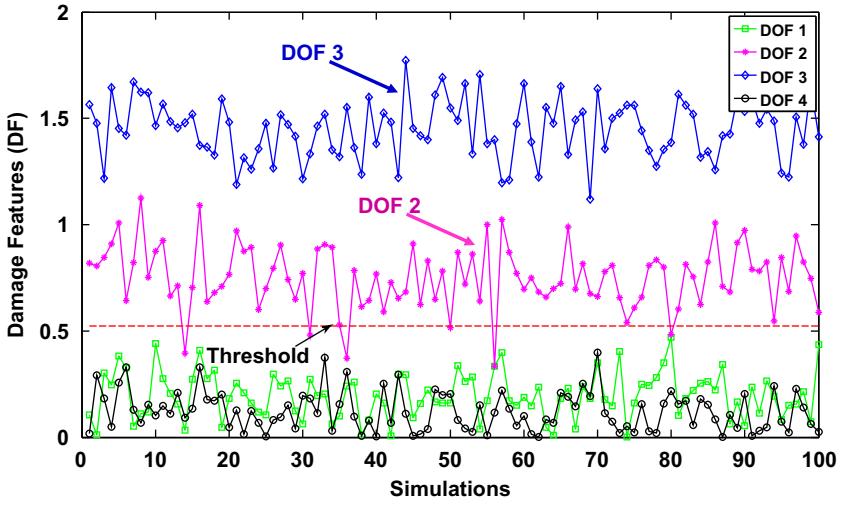

Fig. 5. DFs for each dof for Case 2-1.

4.1.3. Case 2-2: 20% stiffness loss in k_3 (k_3=12), with 10% noise

After showing that damage can be identified and located with noisy data by using Approach II, the stiffness reduction is doubled to see if the severity of the damage can be determined by using the second approach. In this case, the stiffness coefficient between m_2 and m_3 is decreased 20%. Comparing Figs. 5 and 6, the DFs are increased for dofs 2 and 3, which is consistent with the increase in the damage induced to the structure. It is observed that, in addition to existence and location, the severity of the damage can be observed by using the methodology. Also note that, increasing the damage between dofs 2 and 3 did not increase the DFs for dofs 1 and 4 and they are still under the threshold.

4.1.4. Case 2-3: multiple damage case, with 10% noise

This is the final case for the 4 dof system where multiple stiffness reductions are applied to the structure simultaneously to investigate the capability of the methodology to identify multiple damage cases using noisy data. For this case, a 40% stiffness reduction is applied to k_1 (k_1=12) and 20% stiffness reduction is applied to k_3 (k_3=12) at the same time where the noise ratio is 10%. It is clearly apparent from Fig. 7 that the severe damage at the dof 1 is identified and located successfully. Furthermore, the DFs for dofs 2 and 3 are at about the same level with the ones shown in Fig. 6. Also, note that the DFs for dof 1 are almost two times as DFs for dof 3 showing that the severity of the damage is determined successfully, too. Finally, it is observed from the figure that DFs for dof 4 are still under the threshold and very close to zero giving no false positives about dof 4.

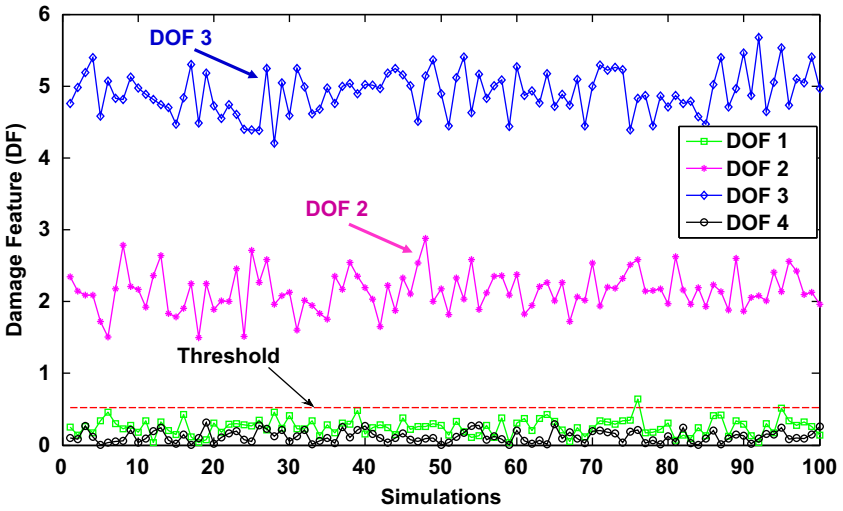

Fig. 6. DFs for each dof for Case 2-2.

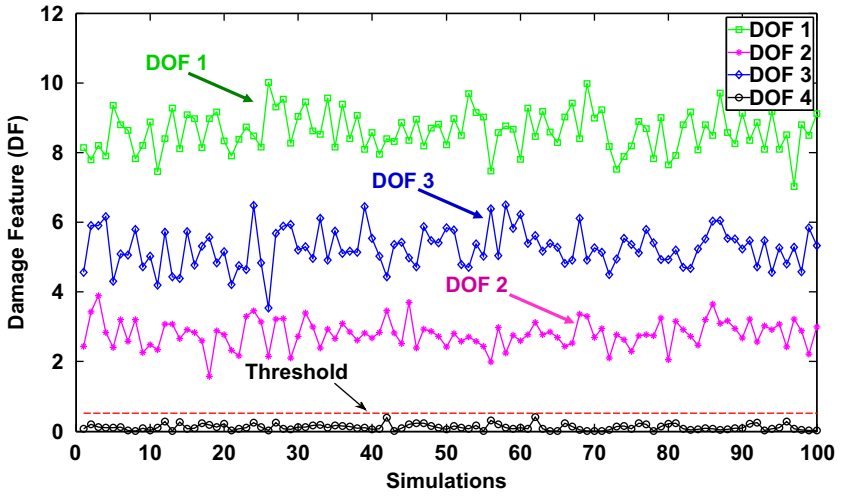

Fig. 7. DFs for each dof for Case 2-3.

4.2. Numerical benchmark problem and experimental studies

4.2.1. Numerical benchmark problem

After showing that Approach II is successfully used to identify the damage induced to the 4 dof numerical model, its capabilities were further investigated using a more complex model and experimental data. First, the numerical model of the first phase of a Bridge Health Monitoring Benchmark Problem was used. The benchmark problem was conducted as a collaborative work by University of Central Florida, University of South Carolina, and Washington University in St. Louis. Details about the benchmark study can be found in Catbas et al. [27] and http://www.cece.ucf.edu/people/catbas/benchmark.htm.

A steel grid model at the University of Central Florida has been selected as the subject for this benchmark problem. This model is a multipurpose specimen enabling researchers to try different methodologies before real life applications. The physical model has two clear spans with continuous beams across the middle supports. The model has two 18 ft (5.49 m) girders in the longitudinal direction. The width of the structure is 3 ft (0.92 m) and the structure is supported by

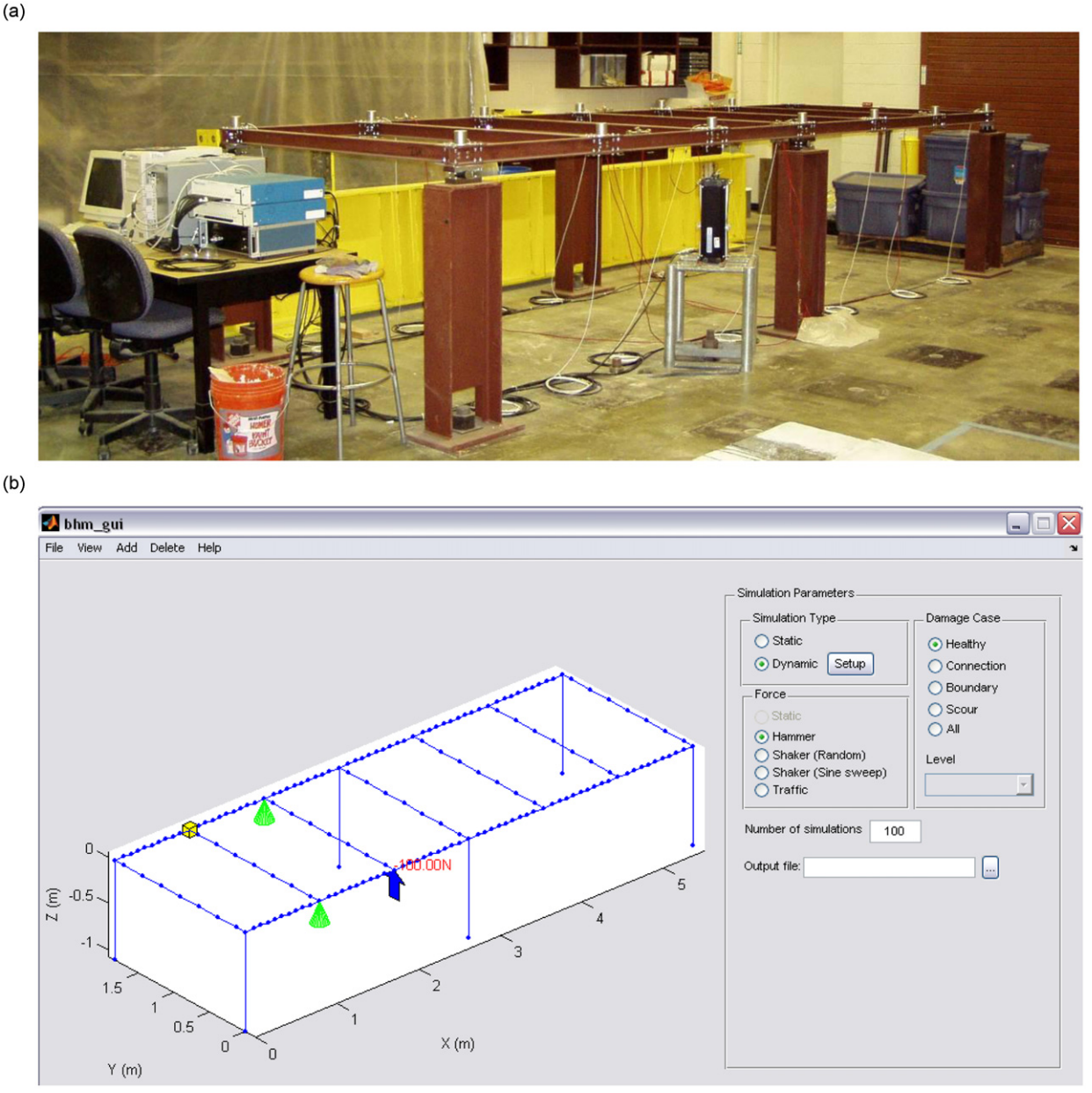

Fig. 8. Benchmark studies (a) the physical model used for the benchmark experiments and (b) the user interface of the numerical benchmark program.

42 in (1.07 m) columns. The test specimen is shown in Fig. 8(a) and more information about the specimen can be found in Catbas et al. [28].

The numerical benchmark problem was prepared by using a detailed finite element (FE) model of the test specimen. The FE model consists of 181 elements, 176 nodes, and 1056 degrees of freedom. A number of different damage cases with different levels can be simulated with the model such as reduced stiffness at connections, boundary condition change and scour. Different types of sensors, such as accelerometers, strain gages, and displacement gages, can be placed on the model to collect static and dynamic data under various loading conditions, e.g. static, impact, random, and traffic loading. Caicedo et al. [29] discusses more details about the numerical model and benchmark study. The user interface of the benchmark program can be seen in Fig. 8(b).

For this part of the study, the numerical model of the benchmark problem is used to verify the methodology. Eight accelerometers are placed on the model to collect the vertical acceleration at all of the corner nodes except supports (N2, N3, N5, N6, N9, N10, N12, and N13 in Fig. 9). The accelerations of the support nodes are not included in the model since they were very close to zero and this created instability in the ARX models. Eight different sensor clusters were created for each reference channel and these clusters are shown in Table 3. The inputs and outputs of the ARX models for each sensor cluster are also shown in Table 3.

4.2.2. Case 3-1: moment release and plate removal at N3, with 10% noise (numerical)

The threshold for the benchmark problem is also calculated as explained in the previous sections. The threshold is calculated as 0.7108. For Case 3-1, the gusset plates at node N3 and the bolts are removed. The free response data is collected from the model and 10% white noise is added artificially. The DFs for this case are calculated and shown in Fig. 10. It is observed that DFs coming from N3, N2, N10, and N5 are higher than the threshold showing us there is a change in the structure around these nodes. Since the DFs for N3 are considerably higher than the other ones, it can be concluded that damage has occurred very close to this node. Also, note that the DFs for N2 are well above the threshold, too. The DFs for N5 and N10 are also above the threshold. This is because these three nodes are the neighbor nodes of N3 (i.e. they are in the same sensor cluster) and removing the gusset plate at N3 affects the stiffness between N2 and N3, N3, and N5; and finally N3 and N10. The highest effect is seen between N2 and N3 since they are on the main girder. Finally, note that the DFs for the other nodes are under the threshold level. Hence, it is evidenced that the methodology is successful at detecting and locating the damage in the benchmark problem for this case without giving any false positives.

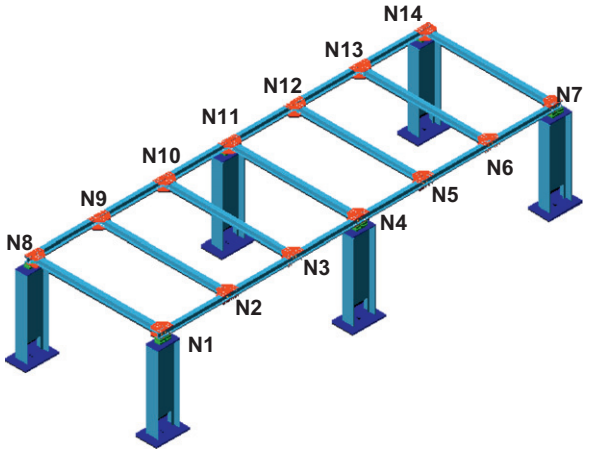

Fig. 9. Node numbers for steel grid structure.

Table 3
The inputs and outputs of the ARX models created for the benchmark problem.

Sensor cluster	Output of the ARX model (reference channel)	Inputs of the ARX model
1	N2	N2, N9, N3
2	N3	N2, N3, N10, N5
3	N5	N3, N5, N12, N6
4	N6	N5, N6, N13
5	N9	N9, N2, N10
6	N10	N9, N10, N3, N12
7	N12	N10, N12, N5, N13
8	N13	N12, N13, N6

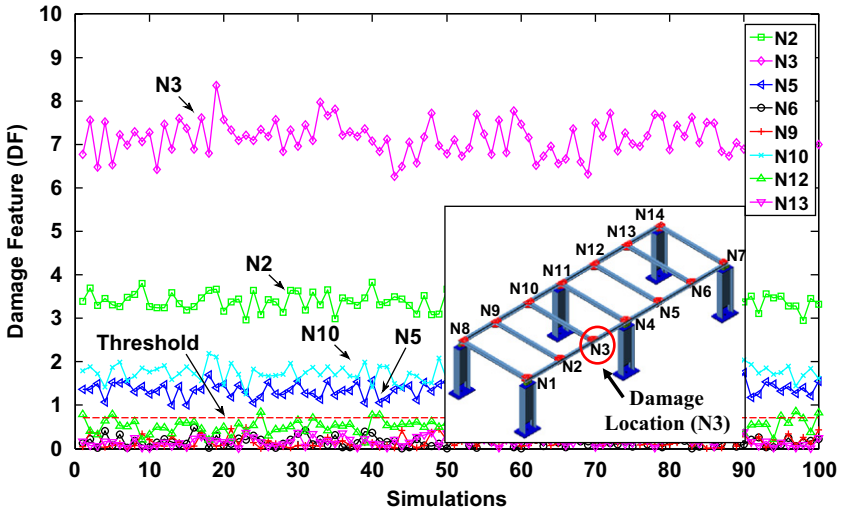

Fig. 10. DFs for Case 3-1 (numerical benchmark).

4.2.3. Case 3-2: boundary restraint at N7 and N14, with 10% noise (numerical)

For this case, a boundary fixity is applied to N7 and N14 simultaneously. Fig. 11(a) shows that the DFs for N6 and N13 are very high and close to each other because they are the closes nodes to the damage location (N7 and N14). It should be re-emphasized here that the data coming from N7 and N14 are not used in the ARX models since they were practically zero. Another observation is that the DFs for N5 and N12 are also very high because they are in the same span with the changed boundary condition. Finally, the nodes in the other span (N2, N3, N9, and N10) are also above threshold since they are affected by the boundary condition change however they are considerably less than the other nodes. Fig. 11(b) clearly shows that N2 and N9 have the smallest DFs since they are the furthest away nodes from the damage location.

4.2.4. Experimental studies

For this part of the study, the experimental data from the steel grid structure in Fig. 8(a) is used. The grid is instrumented with 12 accelerometers in vertical direction at each node (all the nodes except N7–N14 in Fig. 9). The accelerometers used for the experiments are ICP/seismic type accelerometers with a 1000 mV/g sensitivity, 0.01–1200 Hz frequency range, and ∓ 2.5 g of measurement range. To record the dynamic response, an acquisition system from VXI and Agilent Technologies is used. The MTS-Test software package was used for acquisition control of the impact tests. Three different damage scenarios, which are very similar damage cases discussed in the previous section (Cases 3-1 and 3-2), are simulated now experimentally by using the steel grid structure (Fig. 12).

4.2.5. Case 4-1: moment release (bolt removal) at N3 and N10 (experimental)

For Case 4-1, the moment connection of the transverse member at N3 and N10 is released by removing the bolts that are connecting the transverse member to the main girder (Fig. 12). It should be noted that this is a relatively small change since only 16 bolts in a highly complex and redundant structure are removed. The DFs for Case 4-1 are shown in Fig. 13. It is seen from the figure that the DFs for N9, N10, and N3 are higher than the other nodes. This information is showing us that some changes have happened around these nodes. This indeed is the case since the bolts connecting the transverse member to N3 and N10 are removed, which is affecting N9, N10, and N3. The effects should also be seen on N2 and N9 since these are the closest neighbor nodes. Furthermore, a slight change in the DFs of N5 and N12 is also expected since these nodes are also neighbor nodes to N3 and N10. The effect on N9 is clearly apparent from the figure however, the effect on N2 is not observed. Furthermore, the DFs for N12 are higher than the threshold and other nodes. The effect is seen to a lesser extent because there is the support between N10 and N12. One point to note is that the DFs for N2 and N5 are not higher than the other nodes although they are expected to be affected by the applied slight change.

4.2.6. Case 4-2: moment release and plate removal at N3 (experimental)

Case 4-2 is another case to simulate local stiffness loss. The bottom and top gusset plates at node N3 are removed in addition to all bolts at the connection (Fig. 12). However, the bolts or plates at N10 are not removed. Fig. 14 shows that the DFs for N3 is considerably higher than the threshold and other nodes. This increase is due to the plate removal at this node. It is also observed from the figure that the DFs for N2 is also relatively high since N2 is the closest neighbor of N3. Finally the secondary effects of the damage on N5 and N10 are also seen. Therefore, the methodology was very successful at

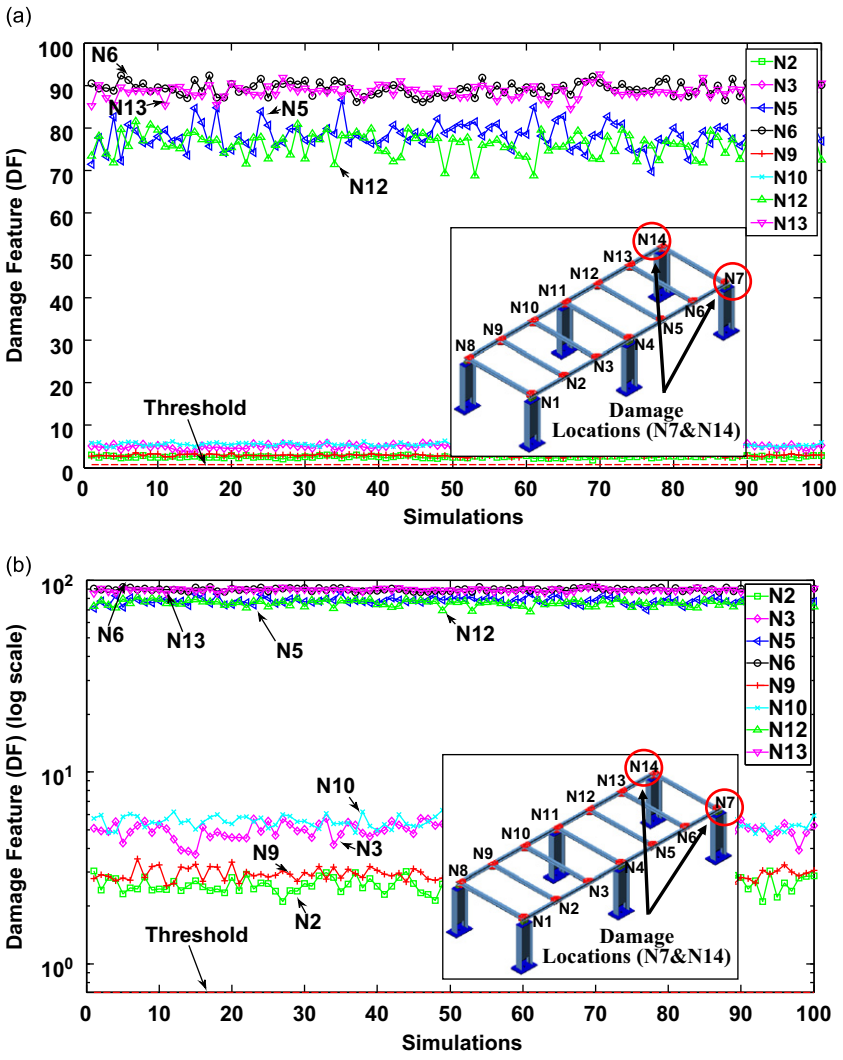

Fig. 11. DFs for Case 3-2 (numerical benchmark) (a) linear scale to show the general view of the DFs and (b) log scale to show the details.

Fig. 12. Experimental damage simulations; bolt removal at N3 and N10 (left), plate removal at N3 for Case 4-2 (center), boundary fixity at N7 and N14 for Case 4-3 (right).

detecting and locating the damage for this experimental damage case. Finally note that the DFs for other nodes are around the threshold showing that these nodes are not significantly affected from the localized damage. Comparison of the results of Case 4-2 with the results of Case 4-1 shows that the values of the DFs are highly correlated with the severity of the damage applied to the structure.

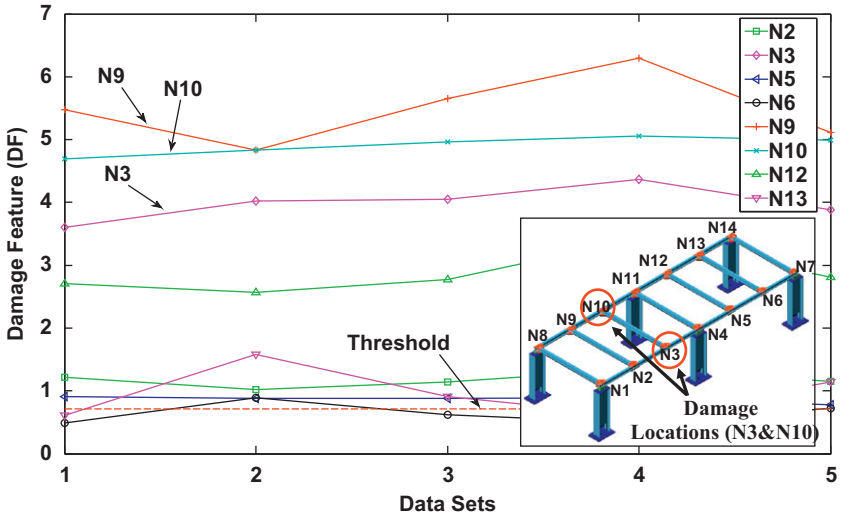

Fig. 13. DFs for Case 4-1 (bolt removal at N3 and N10) using experimental data.

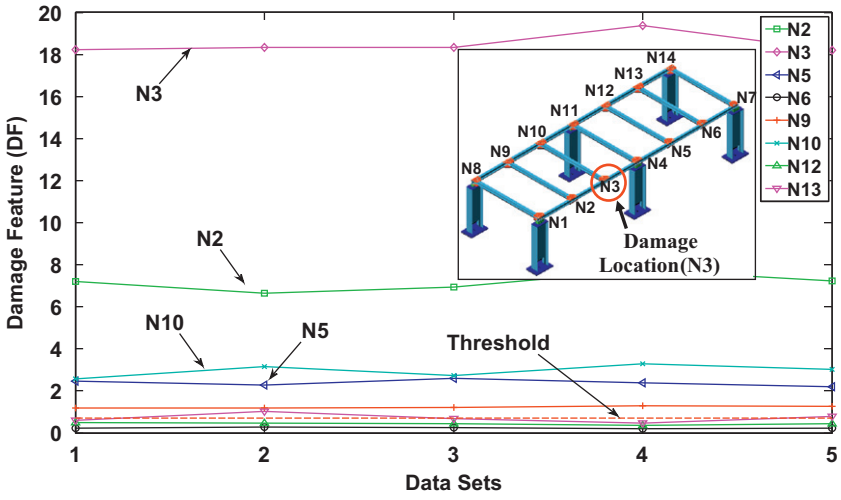

Fig. 14. DFs for Case 4-2 (plate removal at N3) using experimental data.

4.2.7. Case 4-3: boundary restraint at N7 and N14 (experimental)

This damage case is created to simulate some unintended rigidity at a support caused by different reasons such as corrosion. The oversized through-bolts were used at N7 and N14 to introduce fixity at these two supports. The results for this damage case are presented in Fig. 15. It is seen that the DFs for N6 and N13 are considerably higher than the other nodes. This is because these nodes are the closest nodes to the restrained supports (note that N7 and N14 are not instrumented). The DFs for N5 and N12 are also high since they are also affected by the damage. The DFs for the remaining nodes are also slightly higher than the threshold since the structure is changed globally for when boundary changes are applied. Also note that the DFs for N6 and N13 are around 40 indicating that the damage is more severe than Cases 4-1 and 4-2. This information is also very consistent with the severity of the applied damage. Finally, it is observed that DFs for the experimental case presented in Fig. 15 are lower than the numerical counterparts shown in Fig. 11 since a perfect fixity was not realized experimentally by using the oversized bolts unlike the numerical case.

5. Conclusions and discussions

In this study, a new methodology based on time series analysis is presented for damage assessment. It is shown that the proposed approach gives very promising results for detecting, locating and estimating the extent of the damage. In this methodology, ARX models for different sensor clusters are created and different damage features (DFs) are extracted from

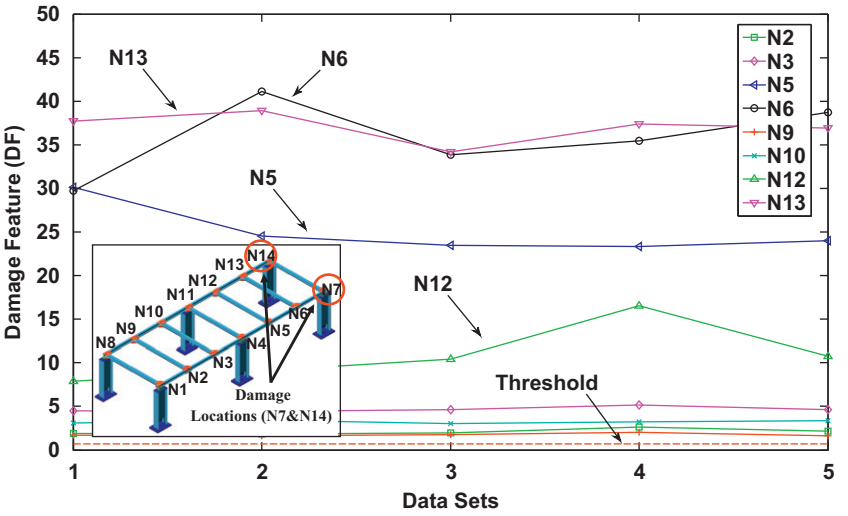

Fig. 15. DFs for Case 4-3 (boundary fixity at N7 and N14) using experimental data.

these models. Two different approaches are introduced where different types of DFs are extracted from the ARX models created for the different clusters.

Approach I is based on direct comparison of the *B* term coefficients of the ARX models. This approach is applied to a 4-dof model for noise-free case and it is shown that it is very successful at giving exact information about the existence, location, and severity of the damage for simple and noise free models. In the second part of the study, Approach II is introduced to consider the effects of the noise and model complexity. For Approach II, the fit ratios of the ARX models are used as the DFs. This approach is applied to a numerical 4 dof model and to numerical data of an international benchmark study. Experimental studies are also conducted for verification of the Approach II. It is demonstrated both with numerical and experimental data that the damage can be identified, located successfully for complex models and test specimens. Furthermore, it is observed that the change in the DFs is a good indicator of the relative increase in the damage extent.

Although the proposed methodology showed great success for the examples under investigation, the authors also acknowledge that the methodology should be verified with more laboratory experiments using different types of structures including plates and shells and field tests before a possible application in real life. The methodology should also be improved for damage detection with ambient vibration data. Finally, the selection of the sensor clusters for 3D sensor layouts should also be addressed in future studies.

Acknowledgements

The authors would like to acknowledge the support from the US Federal Highway Administration (FHWA) Cooperative Agreement Award DTFH61-07-H-00040 as part of the Advanced Explaratory Research Program. Support and feedback from Dr. Hamid Ghasemi of FHWA is greatly appreciated. The opinions and conclusions presented in this paper are those of the authors and do not necessarily reflect the views of the sponsoring organization. The authors would also like to acknowledge Prof Michael Georgiopoulos from Electrical Engineering at University of Central Florida for his feedback and collaboration on statistical pattern recognition algorithms.

References

[1] F.N. Catbas, A.E. Aktan, Condition and damage assessment: issues and some promising indices, *Journal of Structural Engineering—ASCE* 128 (8) (2002) 1026–1036.
[2] S.W. Doebling, C.R. Farrar, M.B. Prime, D.W. Shevitz, Damage identification in structures and mechanical systems based on changes in their vibration characteristics: a detailed literature survey, Los Alamos National Laboratory Report No. LA-13070-MS, Los Alamos, NM, 1996.
[3] H. Sohn, C.R. Farrar, F.M. Hemez, D.D. Shunk, D.W. Stinemates, B.R. Nadler, a review of structural health monitoring literature: 1996–2001, Los Alamos National Laboratory Report, 2003.
[4] K. Worden, Structural fault detection using a novelty measure, *Journal of Sound and Vibration* 201 (1) (1997) 85–101.
[5] P.C. Chang, A. Flatau, S.C. Liu, Review paper: health monitoring of civil infrastructure, *Structural Health Monitoring* 2 (3) (2003) 257–267.
[6] H. Sohn, J.A. Czarnecki, C.R. Farrar, Structural health monitoring using statistical process control, *Journal of Structural Engineering—ASCE* 126 (11) (2000) 1356–1363.
[7] H. Sohn, C.R. Farrar, N.F. Hunter, K. Worden, Structural health monitoring using statistical pattern recognition techniques, *Journal of Dynamic Systems, Measurement, and Control—Transactions of the ASME* 123 (2001) 706–711.
[8] P. Omenzetter, J.M. Brownjohn, Application of time series analysis for bridge monitoring, *Smart Materials and Structures* 15 (2006) 129–138.
[9] Q.W. Zhang, Statistical damage identification for bridges using ambient vibration data, *Computers and Structures* 85 (7–8) (2007) 476–485.

[10] E.P. Carden, J.M. Brownjohn, ARMA modelled time-series classification for structural health monitoring of civil infrastructure, *Mechanical Systems and Signal Processing* 22 (2) (2008) 295–314.
[11] H. Zheng, A. Mita, Two-stage damage diagnosis based on the distance between ARMA models and pre-whitening filters, *Smart Materials and Structures* 16 (2007) 1829–1836.
[12] M. Gul, F.N. Catbas, Statistical pattern recognition for structural health monitoring using time series modeling: theory and experimental verifications, *Mechanical Systems and Signal Processing* 23 (7) (2009) 2192–2204.
[13] S.D. Fassois, S.D. Sakellariou, Time series methods for fault detection and identification in vibrating structures, *Philosophical Transactions of the Royal Society A* 365 (1851) (2007) 411–448.
[14] P. Moyo, J.M.W. Brownjohn, Application of Box–Jenkins models for assessing the effect of unusual events recorded by structural health monitoring systems, *Structural Health Monitoring* 1 (2) (2002) 149–160.
[15] K.K. Nair, A.S. Kiremidjian, Time series based structural damage detection algorithm using Gaussian mixtures modeling, *Journal of Dynamic Systems, Measurement, and Control—Transactions of the ASME* 129 (2007) 285–293.
[16] K.K. Nair, A.S. Kiremidjian, K.H. Law, Time series-based damage detection and localization algorithm with application to the ASCE benchmark structure, *Journal of Sound and Vibration* 291 (1–2) (2006) 349–368.
[17] A. Rytter, *Vibration Based Inspection of Civil Engineering Structures*, Department of Building Technology and Structural Engineering, University of Aalborg, Aalborg, Denmark, 1993.
[18] Y. Lu, F. Gao, A novel time-domain auto-regressive model for structural damage diagnosis, *Journal of Sound and Vibration* 283 (2005) 1031–1049.
[19] E., Monroig, Y. Fujino, Damage identification based on a local physical model for small clusters of wireless sensors, *First Asia-Pacific Workshop on Structural Health Monitoring*, Yokohama, Japan, 2006.
[20] G.E. Box, G.M. Jenkins, G.C. Reinsel, *Time Series Analysis: Forecasting and Control*, Prentice-Hall, New Jersey, 1994.
[21] L. Ljung, *System Identification: Theory for the User*, second ed., Prentice-Hall, Upper Saddle River, NJ, 1999.
[22] S.M. Pandit, S.M. Wu, *Time Series and System Analysis with Applications*, Krieger Pub. Co, Malabar, FL, 1993.
[23] M., Gul, F.N. Catbas, A new methodology for identification, localization and quantification of damage by using time series modeling, *26th International Modal Analysis Conference (IMAC XXVI)*, Orlando, FL, 2008.
[24] H. Lus, M. De Angelis, R. Betti, A new approach for reduced order modeling of mechanical systems using vibration measurements., *Journal of Applied Mechanics* (2003) 715–72370 (2003) 715–723.
[25] M. Gul, F.N. Catbas, A modified time series analysis for identification, localization, and quantification of damage, *27th International Modal Analysis Conference (IMAC XXVII)*, Orlando, FL, 2009.
[26] K. Worden, G. Manson, N.R.J. Fieller, Damage detection using outlier analysis, *Journal of Sound and Vibration* 229 (3) (2000) 647–667.
[27] F.N. Catbas, J.M. Caicedo, S.J. Dyke, Development of a Benchmark problem for bridge health monitoring, *Proceedings of the International Conference on Bridge Maintenance, Safety and Management*, *IABMAS*, Porto, Portugal, 2006.
[28] F.N. Catbas, M. Gul, J.L. Burkett, Damage assessment using flexibility and flexibility-based curvature for structural health monitoring, *Smart Materials and Structures* 17 (1) (2008) 015024 (12 pp).
[29] J.M. Caicedo, F.N. Catbas, M. Gul, R. Zaurin, Phase I of the benchmark problem for bridge health monitoring: numerical data, *Proceedings of the 18th Engineering Mechanics Division Conference of the ASCE*, Virginia Tech, Blacksburg, VA, 2007.